# Emergence of a diverse array of phases in an exactly solvable model

Zhipeng Sun[1,*] and Hai-Qing Lin[1,2,†]
[1]*Beijing Computational Science Research Center, Beijing 100193, China*
[2]*Department of Physics, Zhejiang University, Hangzhou 310027, China*

(Received 28 October 2023; revised 29 January 2024; accepted 20 February 2024; published 5 March 2024)

Numerical solvers for strongly correlated electronic systems poses a significant challenge in condensed matter theory. In recent years, extensive exploration of strongly correlated effects has been carried out based on exactly solvable Hatsugai-Kohmoto-like models. In this work, we investigate a simple two-site cluster extension of the Hatsugai-Kohmoto model. The model exhibits a rich variety of phases, including the charge-4$e$ phase, charge-2$e$ phase, metallic phase, pseudogap phase, and Luttinger liquid phase. These findings contribute to the understanding of strongly correlated physics and superconducting physics.

DOI: 10.1103/PhysRevB.109.115108

## I. INTRODUCTION

Correlated electronic systems exhibit numerous intriguing phenomena, such as metal-insulator transition [1,2], strange metal behavior [3–6], and high-temperature superconductivity [7–9]. These effects are believed to be captured by the Hubbard model and its extensions [10–15], yet they cannot be described by the traditional Ginzburg-Landau framework and remain challenging to solve. Despite the development of numerous numerical methods over years, however, our understanding of the seemingly simple two-dimensional (2D) Hubbard model is still lacking. Determinantal quantum Monte Carlo simulations [16–18] can efficiently provide numerically accurate results in the half-filled case, but it faces challenges in scenarios away from half-filling due to the sign problem. Density matrix renormalization group methods [19–21] perform well in one-dimensional and quasi-one-dimensional systems but struggle in two-dimensional situations due to area laws for the entanglement entropy [22]. Dynamical mean-field theory [23–25] is exact in infinite dimensions but faces difficulties capturing nonlocal correlations in low-dimensional cases. In short, the development of numerical methods for strongly correlated electronic systems is urgently needed and presents a challenging task.

Therefore, seeking insights into strongly correlated physics from exactly solvable models might be a wise and fruitful avenue. For instance, a simple and exactly solvable model proposed by Hatsugai and Kohmoto [26] in 1992 proves illustrative. The Hamiltonian simply takes the form $\hat{H} = \sum_{\boldsymbol{k}} \hat{H}_{\boldsymbol{k}}$, where $\hat{H}_k = \sum_{\alpha=\uparrow,\downarrow}(\varepsilon_{\boldsymbol{k}} - \mu)\hat{n}_{\alpha,\boldsymbol{k}} + U\hat{n}_{\uparrow,\boldsymbol{k}}\hat{n}_{\downarrow,\boldsymbol{k}}$ and $\hat{n}_{\alpha,\boldsymbol{k}}$ is the number operator with $z$ spin $\alpha$ and quasimomentum $\boldsymbol{k}$. This model is easy to solve, yet it does capture some crucial physics of the Hubbard model: when $U < 0$, the ground state exhibits electronic pairing, relating to the superconductivity; and when $U$ exceeds half of the bandwidth an insulating phase emerges at half-filling, relating to the Mott insulator. In recent years, the Hatsugai-Kohmoto (HK) model has garnered significant attention and has been subject to further extensions [27–48].

In this work, we introduce a two-site cluster extension of the HK model. The Hamiltonian retains the simple form $\hat{H} = \sum_{\boldsymbol{k}} \hat{H}_{\boldsymbol{k}}$, while $\hat{H}_{\boldsymbol{k}}$ becomes slightly more intricate. In the HK model, $\hat{H}_{\boldsymbol{k}=0}$ corresponds to the Hubbard model on one site, whereas in our model, it corresponds to the extended Hubbard model ($t$-$U$-$V$ model) on two sites. We observe that the ground state of this model exhibits a rich variety of phases, including the charge-4$e$ phase, charge-2$e$ phase, metallic phase, pseudogap phase, and Luttinger liquid phase. These findings contribute to advancing our understanding of strongly correlated physics and superconducting physics.

This paper is organized as follows. In Sec. II, we present the exact solution of the two-site $t$-$U$-$V$ model, constructing an exactly solvable model, and briefly showcased possible ground state phases. Next in Sec. III, we provide the quantum phase diagram at quarter-filling and analyze these phases. Finally in Sec. IV, we make a summary and outlook.

## II. TWO-SITE CLUSTER EXTENSION

From the work of Hatsugai and Kohmoto, it is straightforward to draw a conclusion: if the Hamiltonian takes the form $\hat{H} = \sum_{\boldsymbol{k}} \hat{H}_{\boldsymbol{k}}$, where $\hat{H}_{\boldsymbol{k}}$ can be exactly solved, then $\hat{H}$ is also exactly solvable. Note that $\hat{H}_{\boldsymbol{k}}$'s are mutually commuting with each other. Let $\hat{H}_{\boldsymbol{k}}|\varphi_{\boldsymbol{k}}\rangle = h_{\boldsymbol{k}}|\varphi_{\boldsymbol{k}}\rangle$, and one obtains $\hat{H}|\Psi\rangle = E|\Psi\rangle$, where

$$|\Psi\rangle = \otimes_{\boldsymbol{k}}|\varphi_{\boldsymbol{k}}\rangle, \text{ and } E = \sum_{\boldsymbol{k}} h_{\boldsymbol{k}}. \tag{1}$$

With this property, the ground state and thermodynamics of the system governed by the Hamiltonian $\hat{H}$ can be easily obtained.

In the HK model, $H_{\boldsymbol{k}=0}$ simply corresponds to the Hubbard model on one site. To enrich its physics, we introduce some complexity to $\hat{H}_{\boldsymbol{k}}$—now $\hat{H}_{\boldsymbol{k}=0}$ corresponds to the $t$-$U$-$V$ model

*zpsun@csrc.ac.cn
†haiqing0@csrc.ac.cn

 

TABLE I. Eigenvalues and eigenstates of the two-site Hamiltonian.

| Occupancy | Eigenvalue | Eigenstate |
|---|---|---|
| $N=0$ | $E_{0,0}=0$ | $\|\Omega\rangle$ |
| | $E_{1,0}=-t-3\lambda_0+\lambda_\pi-\mu$ | $\hat{c}^\dagger_{\uparrow,0}\|\Omega\rangle$, $\hat{c}^\dagger_{\downarrow,0}\|\Omega\rangle$ |
| $N=1$ | $E_{1,\pi}=t-\mu-3\lambda_0+\lambda_\pi$ | $\hat{c}^\dagger_{\uparrow,\pi}\|\Omega\rangle$, $\hat{c}^\dagger_{\downarrow,\pi}\|\Omega\rangle$ |
| $N=2$ | $E_{2,\pi,\mathrm{t}}=-4\lambda_0-2\mu$ | $\frac{1}{\sqrt{2}}(\hat{c}^\dagger_{\uparrow,0}\hat{c}^\dagger_{\downarrow,\pi}-\hat{c}^\dagger_{\uparrow,\pi}\hat{c}^\dagger_{\downarrow,0})\|\Omega\rangle$, |
| | | $\hat{c}^\dagger_{\uparrow,0}\hat{c}^\dagger_{\uparrow,\pi}\|\Omega\rangle$, $\hat{c}^\dagger_{\downarrow,0}\hat{c}^\dagger_{\downarrow,\pi}\|\Omega\rangle$ |
| | $E_{2,\pi,\mathrm{s}}=-4\lambda_0+4\lambda_\pi-2\mu$ | $\frac{1}{\sqrt{2}}(\hat{c}^\dagger_{\uparrow,0}\hat{c}^\dagger_{\downarrow,\pi}+\hat{c}^\dagger_{\uparrow,\pi}\hat{c}^\dagger_{\downarrow,0})\|\Omega\rangle$ |
| | $E_{2,0,-}=-4\lambda_0+2\lambda_\pi-2\sqrt{t^2+\lambda_\pi^2}-2\mu$ | $(\cos\theta\hat{c}^\dagger_{\uparrow,0}\hat{c}^\dagger_{\downarrow,0}-\sin\theta\hat{c}^\dagger_{\uparrow,\pi}\hat{c}^\dagger_{\downarrow,\pi})\|\Omega\rangle$ |
| | $E_{2,0,+}=-4\lambda_0+2\lambda_\pi+2\sqrt{t^2+\lambda_\pi^2}-2\mu$ | $(\sin\theta\hat{c}^\dagger_{\uparrow,0}\hat{c}^\dagger_{\downarrow,0}+\cos\theta\hat{c}^\dagger_{\uparrow,\pi}\hat{c}^\dagger_{\downarrow,\pi})\|\Omega\rangle$ |
| $N=3$ | $E_{3,0}=t-3\lambda_0+\lambda_\pi-3\mu$ | $\hat{c}^\dagger_{\uparrow,\pi}\hat{c}^\dagger_{\downarrow,0}\hat{c}^\dagger_{\downarrow,\pi}\|\Omega\rangle$, $\hat{c}^\dagger_{\uparrow,0}\hat{c}^\dagger_{\uparrow,\pi}\hat{c}^\dagger_{\downarrow,\pi}\|\Omega\rangle$ |
| | $E_{3,\pi}=-t-3\lambda_0+\lambda_\pi-3\mu$ | $\hat{c}^\dagger_{\uparrow,0}\hat{c}^\dagger_{\uparrow,\pi}\hat{c}^\dagger_{\downarrow,0}\|\Omega\rangle$, $\hat{c}^\dagger_{\uparrow,0}\hat{c}^\dagger_{\downarrow,0}\hat{c}^\dagger_{\downarrow,\pi}\|\Omega\rangle$ |
| $N=4$ | $E_{4,0}=-4\mu$ | $\hat{c}^\dagger_{\uparrow,0}\hat{c}^\dagger_{\uparrow,\pi}\hat{c}^\dagger_{\downarrow,0}\hat{c}^\dagger_{\downarrow,\pi}\|\Omega\rangle$ |

on two sites instead. In the text below, we will first demonstrate the fundamental physics of the two-site model.

### A. Two-site *t*-*U*-*V* model

The Hamiltonian of the two-site *t*-*U*-*V* model reads

$$\hat{H}_0 = -t\sum_{\alpha}(\tilde{c}^\dagger_{\alpha,A}\tilde{c}_{\alpha,B}+\tilde{c}^\dagger_{\alpha,B}\tilde{c}_{\alpha,A})-\tilde{\mu}\sum_{\alpha,\iota}\tilde{n}_{\alpha,\iota} + U\sum_{\iota}\tilde{n}_{\uparrow,\iota}\tilde{n}_{\downarrow,\iota}+V\sum_{\alpha,\alpha'}\tilde{n}_{\alpha,A}\tilde{n}_{\alpha',B}. \tag{2}$$

Here $\tilde{c}_{\alpha,\iota}$ is the annihilation operator for the electron with $z$ spin $\alpha$ on site $\iota$ ($A$ or $B$). $t\geqslant 0$ is the hopping strength, $U$ is the on-site interaction strength, $V$ is the intersite interaction strength, and $\tilde{\mu}$ is the chemical potential.

By introducing the transformations

$$\tilde{c}_{\alpha,A}=\frac{1}{\sqrt{2}}(\hat{c}_{\alpha,0}+\hat{c}_{\alpha,\pi}),\ \tilde{c}_{\alpha,B}=\frac{1}{\sqrt{2}}(\hat{c}_{\alpha,0}-\hat{c}_{\alpha,\pi}), \tag{3}$$

we can rewrite the two-site Hamiltonian in the momentum representation:

$$\hat{H}_0 = -t\sum_{\alpha}(\hat{n}_{\alpha,0}-\hat{n}_{\alpha,\pi})-(\mu+4\lambda_0)\hat{\rho}_0 + \lambda_0\hat{\rho}_0^2+\lambda_\pi\hat{\rho}_\pi^2. \tag{4}$$

Here $\mu=\tilde{\mu}+U/2-4\lambda_0$ is a shifted chemical potential and will be used in text below. The coupling strengths $\lambda_0$ and $\lambda_\pi$ are determined by the relationships $U/2=\lambda_0+\lambda_\pi$ and $V/2=\lambda_0-\lambda_\pi$. The two operators $\hat{\rho}_0$ and $\hat{\rho}_\pi$ are defined as:

$$\hat{\rho}_0=\sum_{\alpha,q=0,\pi}\hat{c}^\dagger_{\alpha,q}\hat{c}_{\alpha,q},\ \hat{\rho}_\pi=\sum_{\alpha,q=0,\pi}\hat{c}^\dagger_{\alpha,q+\pi}\hat{c}_{\alpha,q}. \tag{5}$$

The two-site Hamiltonian Eq. (4) can be easily solved; its 16 eigenstates together with the 10 eigenvalues are presented in Table I, in which $\theta\in[-\pi/4,\pi/4]$ is determined by $\tan 2\theta=\lambda_\pi/t$. It is easy to observe that the ground-state energy can only be one of the five possibilities: $E_{0,0}$, $E_{1,0}$, $E_{2,0,-}$, $E_{3,\pi}$, or $E_{4,0}$. Let $E_i$ be the minimum eigenvalue with specific occupation number $i$, for $i=0,1,2,3,4$. Then

$$E_0=0, \tag{6a}$$
$$E_1=-t-3\lambda_0+\lambda_\pi-\mu, \tag{6b}$$
$$E_2=-4\lambda_0+2\lambda_\pi-2\sqrt{t^2+\lambda_\pi^2}-2\mu, \tag{6c}$$
$$E_3=-t-3\lambda_0+\lambda_\pi-3\mu, \tag{6d}$$
$$E_4=-4\mu. \tag{6e}$$

The occupation number $N$ of the ground state can be determined by minimizing $E_N$. The variation of $N$ in the $\lambda_0$-$\mu$ plane is sketched in Fig. 1. The colored regions stand for different $N$'s, gray for $N=0$, blue for $N=1$, green for $N=2$, orange for $N=3$, and brown for $N=4$. The solid lines are boundary of two different regions, and their equations are $E_{N,\min}=E_{N',\min}$ with $N$ and $N'$ the occupation numbers. The specific

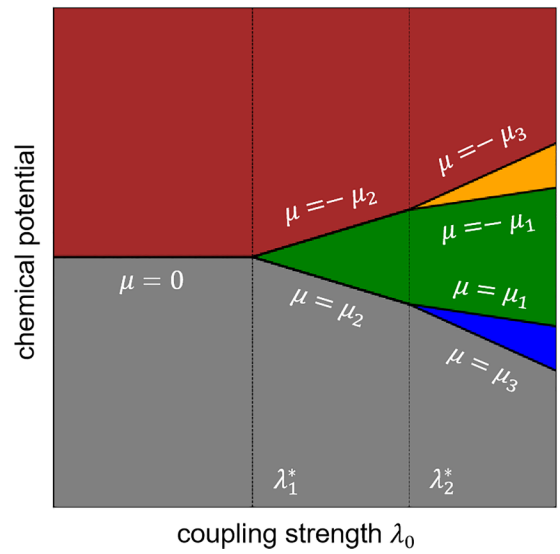


FIG. 1. The occupation number for the two-site Hamiltonian in the $\lambda_0$-$\mu$ plane.

equations are $\mu = 0$, $\mu = \pm\mu_1$, $\mu = \pm\mu_2$, and $\mu = \pm\mu_3$, with the expressions

$$\mu_1 = -\lambda_0 + \lambda_\pi - 2\sqrt{t^2 + \lambda_\pi^2} + t, \tag{7a}$$

$$\mu_2 = -2\lambda_0 + \lambda_\pi - \sqrt{t^2 + \lambda_\pi^2}, \tag{7b}$$

$$\mu_3 = -3\lambda_0 + \lambda_\pi - t. \tag{7c}$$

The dashed lines indicate where three different regions intersect, and their equations are $\lambda_0 = \lambda_1^*$ and $\lambda_0 = \lambda_2^*$, where

$$\lambda_1^* = \tfrac{1}{2}\big(\lambda_\pi - \sqrt{t^2 + \lambda_\pi^2}\big), \tag{8a}$$

$$\lambda_2^* = \sqrt{t^2 + \lambda_\pi^2} - t. \tag{8b}$$

Note that $\lambda_1^* < 0 < \lambda_2^*$ if both $t$ and $\lambda_\pi$ are nonzero.

Under different parameter conditions, the possible values of the occupation number vary. When $\lambda_0 < \lambda_1^*$, the possible values are 0 and 4, implying the formation of a bound state with four electrons, referred to as a quartet. When $\lambda_1^* < \lambda_0 < \lambda_2^*$, the possible values are 0, 2, and 4, indicating the pairing of two electrons. When $\lambda_0 > \lambda_2^*$ the minimum increment is one, signifying the absence of bound state. In these three scenarios, we refer to the minimum unit of the two-site cluster as quartet, pair, and electron, respectively.

### B. Lattice model and its ground states

Now, let us consider such a somewhat impractical system, which is composed of independent $\boldsymbol{k}$ blocks, each of which is a two-site cluster with different parameters $(t, \lambda_0, \lambda_\pi)$. Here, we regard $\boldsymbol{k}$ as the momentum in the half of the first Brillouin zone and assume that $t$ depends on $\boldsymbol{k}$ and lies in the range $[0, W]$, while $\lambda_0$ and $\lambda_\pi$ are constants. The Hamiltonian of the whole system then takes the form $\hat{H} = \sum_{\boldsymbol{k}} \hat{H}_{\boldsymbol{k}}$ with

$$\begin{aligned}\hat{H}_{\boldsymbol{k}} = &-t_{\boldsymbol{k}}(\hat{n}_{\uparrow,\boldsymbol{k}} - \hat{n}_{\uparrow,\boldsymbol{\pi}+\boldsymbol{k}} + \hat{n}_{\downarrow,\boldsymbol{k}} - \hat{n}_{\downarrow,\boldsymbol{\pi}-\boldsymbol{k}}) \\ &- (\mu + 4\lambda_0)\hat{\rho}_{0,\boldsymbol{k}} + \lambda_0\hat{\rho}_{0,\boldsymbol{k}}^2 + \lambda_\pi\hat{\rho}_{\pi,\boldsymbol{k}}^2.\end{aligned} \tag{9}$$

Here the operators $\hat{\rho}_{0,\boldsymbol{k}}$ and $\hat{\rho}_{\pi,\boldsymbol{k}}$ are given by

$$\hat{\rho}_{0,\boldsymbol{k}} = \sum_{\boldsymbol{q}=\boldsymbol{0},\boldsymbol{\pi}} \hat{c}_{\uparrow,\boldsymbol{q}+\boldsymbol{k}}^\dagger \hat{c}_{\uparrow,\boldsymbol{q}+\boldsymbol{k}} + \hat{c}_{\downarrow,\boldsymbol{q}-\boldsymbol{k}}^\dagger \hat{c}_{\downarrow,\boldsymbol{q}-\boldsymbol{k}}, \tag{10a}$$

$$\hat{\rho}_{\pi,\boldsymbol{k}} = \sum_{\boldsymbol{q}=\boldsymbol{0},\boldsymbol{\pi}} \hat{c}_{\uparrow,\boldsymbol{q}+\boldsymbol{\pi}+\boldsymbol{k}}^\dagger \hat{c}_{\uparrow,\boldsymbol{q}+\boldsymbol{k}} + \hat{c}_{\downarrow,\boldsymbol{q}+\boldsymbol{\pi}-\boldsymbol{k}}^\dagger \hat{c}_{\downarrow,\boldsymbol{q}-\boldsymbol{k}}. \tag{10b}$$

The Hamiltonian $\hat{H}_{\boldsymbol{k}}$ can be regarded as replacements to $\hat{H}_0$ as follows: $\hat{c}_{\uparrow,q}$ is replaced by $\hat{c}_{\uparrow,\boldsymbol{q}+\boldsymbol{k}}$, $\hat{c}_{\downarrow,q}$ is replaced by $\hat{c}_{\downarrow,\boldsymbol{q}-\boldsymbol{k}}$, and $t$ is replaced by $t_{\boldsymbol{k}}$. Results about $\hat{H}_0$ can be directly carried over to $\hat{H}_{\boldsymbol{k}}$, as long as $t$ is replaced by $t_{\boldsymbol{k}}$. Below, we will consider $E_N$ defined by Eq. (6), $\mu_i$ defined by Eq. (7), and $\lambda_1^*$ and $\lambda_2^*$ defined by Eq. (8), all as functions of $t$.

As mentioned above, the lattice model is exactly solvable. Here, we focus on its ground state. When $|\Psi\rangle$ [see Eq. (1)] is the ground state of $\hat{H}$, every $|\varphi_{\boldsymbol{k}}\rangle$ should be the ground state of $\hat{H}_{\boldsymbol{k}}$.

It would be convenient to introduce the effective dispersion $\xi_{\boldsymbol{k},i}$ $(i = 1, 2, 3, 4)$ as follows. When $\lambda_0 < \lambda_1^*(t_{\boldsymbol{k}})$, the minimum unit in the $\boldsymbol{k}$ block is the quartet, and we define $\xi_{\boldsymbol{k},i} = -\mu$ for $i = 1, 2, 3, 4$, which stands for the energy per electron in the quartet. When $\lambda_0$ lies in the range between $\lambda_1^*(t_{\boldsymbol{k}})$ and $\lambda_2^*(t_{\boldsymbol{k}})$, the minimum unit in the $\boldsymbol{k}$ block is the pair, and we define $\xi_{\boldsymbol{k},1} = \xi_{\boldsymbol{k},2} = \mu_2(t_{\boldsymbol{k}}) - \mu$ and $\xi_{\boldsymbol{k},3} = \xi_{\boldsymbol{k},4} = -\mu_2(t_{\boldsymbol{k}}) - \mu$, which, respectively, represent the energy per electron in the first pair and the second pair. When $\lambda_0 > \lambda_2^*(t_{\boldsymbol{k}})$, the minimum unit in the $\boldsymbol{k}$ block is the electron, and we define $\xi_{\boldsymbol{k},i} = E_{\boldsymbol{k},i} - E_{\boldsymbol{k},i-1}$. By this definition, the occupation number in the $\boldsymbol{k}$ block can be easily determined; it equals to the maximum $i$ that satisfies $\xi_{\boldsymbol{k},i} \leqslant 0$.

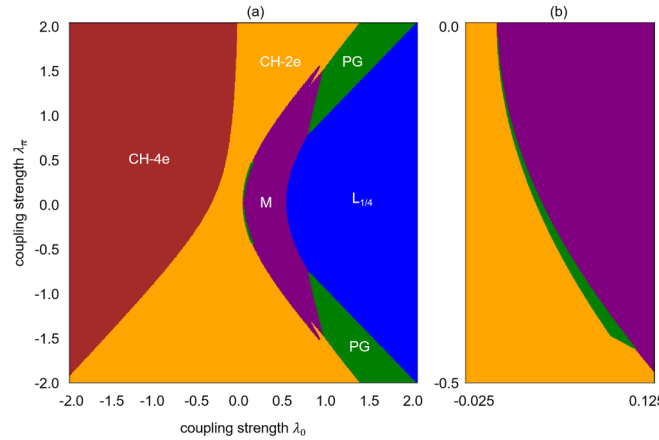


FIG. 2. Quantum phase diagram at quarter filling in one-dimensional case, (a) for $\lambda_0/W \in (-2.0, 2.0)$ and $\lambda_\pi/W \in (-2.0, 2.0)$; (b) for $\lambda_0/W \in (-0.025, 0.125)$ and $\lambda_\pi/W \in (-0.5, 0)$.

The surface defined by the set of $\boldsymbol{k}$ points that satisfy $\xi_{\boldsymbol{k},i} = 0$ is important for the physical properties, and we refer to it as the zero-energy surface. In the absence of interactions, the zero-energy surface is identical to the well-known Fermi surface. Based on the minimum units at the zero-energy surface, we can categorize the ground state into five phases: (i) When the zero-energy surface is absent, the system is in a Luttinger liquid phase (as explained below). (ii) When only electrons exist on the zero-energy surface, the system is in a metallic phase. (iii) When only pairs exist on the zero-energy surface, the system is in a charge-2$e$ phase. (iv) When only quartets exist on the zero-energy surface, the system is in a charge-4$e$ phase. (v) In a special case, when both electrons and pairs coexist on the zero-energy surface, we refer to the system as being in a pseudogap phase (see Ref. [30]).

## III. PROPERTIES OF GROUND-STATE PHASES

We present the quantum phase diagram at quarter-filling in one-dimensional case in Fig. 2. Here, the brown regime denotes the charge-4$e$ phase (CH-4$e$), the orange regime denotes the charge-2$e$ phase (CH-2$e$), the purple regime denotes the metallic phase (M), the purple regime denotes the pseudogap phase (PG), and the blue regime denotes the quarter-filled Luttinger liquid phase ($L_{1/4}$). For uncertain fillings, we present the phases that may occur under different parameter conditions in Table II, where $L_{1/2}$ represents for the half-filled Luttinger liquid phase.

The charge-4$e$ phase occurs at $\mu = 0$ in the case $\lambda_0 < \lambda_1^*(0)$. When $\lambda_0 < \lambda_1^*(W)$, the minimum units in all $\boldsymbol{k}$ blocks are quartets. At $\mu = 0$, the energy of each quartet is zero,

TABLE II. Possible phases at different parameters.

| Parameter | Minimum Units | Possible Phases |
|---|---|---|
| $\lambda_0 < \lambda_1^*(W)$ | quartet | CH-4$e$ |
| $\lambda_1^*(W) \leqslant \lambda_0 < \lambda_1^*(0)$ | quartet, pair | CH-4$e$, CH-2$e$ |
| $\lambda_1^*(0) \leqslant \lambda_0 < \lambda_2^*(W)$ | pair | CH-2$e$, $L_{1/2}$ |
| $\lambda_2^*(W) \leqslant \lambda_0 < \lambda_2^*(0)$ | pair, electron | CH-2$e$, M, PG, $L_{1/2}$ |
| $\lambda_0 \geqslant \lambda_2^*(0)$ | electron | M, $L_{1/4}$, $L_{1/2}$ |

meaning their presence or absence does not affect the total energy of the whole system. The ground state can be expressed as

$$|\Psi\rangle = \sum_{\boldsymbol{k}} (u_{\boldsymbol{k}} + v_{\boldsymbol{k}} \hat{c}^\dagger_{\uparrow,\boldsymbol{k}} \hat{c}^\dagger_{\uparrow,\boldsymbol{\pi}+\boldsymbol{k}} \hat{c}^\dagger_{\downarrow,-\boldsymbol{k}} \hat{c}^\dagger_{\downarrow,\boldsymbol{\pi}-\boldsymbol{k}})|\Omega\rangle, \tag{11}$$

for arbitrary $u_{\boldsymbol{k}}$, $v_{\boldsymbol{k}}$ satisfying $|u_{\boldsymbol{k}}|^2 + |v_{\boldsymbol{k}}|^2 = 1$.

When $\lambda_1^*(W) < \lambda_0 < \lambda_1^*(0)$, the minimum units in $\boldsymbol{k}$ blocks are quartets (for $t_{\boldsymbol{k}} \leqslant t^*$) and pairs (for $t_{\boldsymbol{k}} > t^*$), where $t^*$ is determined by $\lambda_0 = \lambda_1^*(t^*)$. The ground state is then given by

$$|\Psi\rangle = \prod_{t_{\boldsymbol{k}} \leqslant t^*} (u_{\boldsymbol{k}} + v_{\boldsymbol{k}} \hat{c}^\dagger_{\uparrow,\boldsymbol{k}} \hat{c}^\dagger_{\uparrow,\boldsymbol{\pi}+\boldsymbol{k}} \hat{c}^\dagger_{\downarrow,-\boldsymbol{k}} \hat{c}^\dagger_{\downarrow,\boldsymbol{\pi}-\boldsymbol{k}})|\Phi\rangle, \tag{12}$$

where

$$|\Phi\rangle \equiv \prod_{t_{\boldsymbol{k}} > t^*} \hat{d}^\dagger_{\boldsymbol{k}} |\Omega\rangle, \tag{13}$$

with

$$\hat{d}^\dagger_{\boldsymbol{k}} = \cos\theta_{\boldsymbol{k}} \hat{c}^\dagger_{\uparrow,\boldsymbol{k}} \hat{c}^\dagger_{\downarrow,-\boldsymbol{k}} - \sin\theta_{\boldsymbol{k}} \hat{c}^\dagger_{\uparrow,\boldsymbol{\pi}+\boldsymbol{k}} \hat{c}^\dagger_{\downarrow,\boldsymbol{\pi}-\boldsymbol{k}}. \tag{14}$$

Here $\theta_{\boldsymbol{k}} \in [-\pi/4, \pi/4]$ is determined by $\tan 2\theta_{\boldsymbol{k}} = \lambda_\pi / t_{\boldsymbol{k}}$.

The charge-4$e$ phase may be relevant to the concept of recently popularized charge-4$e$ superconductors [49–59]. Experimental evidence has indicated the existence of charge-4$e$ and even 6$e$ superconductivity [58], although these experimental findings may also be explained by other mechanisms. Theoretical studies often employ a Hamiltonian with charge $U(1)$ symmetry breaking [53] to investigate the properties of the charge-4$e$ superconductors. In contrast, our starting point is a Hamiltonian preserving the charge $U(1)$ symmetry, which may lend additional significance to this research.

The charge-2$e$ phase, in which only pairs exist on the zero-energy surface, occurs only when $\lambda_1^*(0) < \lambda_0 < \lambda_2^*(0)$. The typical state is given by

$$|\Psi\rangle = \prod_{t_{\boldsymbol{k}} \geqslant t_{2,0}} \hat{d}^\dagger_{\boldsymbol{k}} |\Omega\rangle, \tag{15}$$

where $\mu_2(t_{2,0}) = \mu$ and $t_{2,0} \neq 0$. Here $\boldsymbol{k}$ blocks with $t_{\boldsymbol{k}} \geqslant t_{2,0}$ are doubly occupied, and $\boldsymbol{k}$ blocks with $t_{\boldsymbol{k}} < t_{2,0}$ are empty.

Despite the presence of pairs in the charge-2$e$ phase, it should not be considered a true superconducting state due to lacking of phase coherence. To exhibit superconductivity, additional terms may be necessary, as seen in the HK-BCS model [35,36] and the Richardson-Gaudin models [60].

The metallic phase, in which only electrons exist on the zero-energy surface, occurs only when $\lambda_0 > \lambda_2^*(W)$. As for the pseudogap phase, in which electrons and pairs coexist on the zero-energy surface, it occurs only when $\lambda_2^*(W) < \lambda_0 < \lambda_2^*(0)$. The single-particle spectrum is gapless on the surface where electrons are present, while it exhibits a gap on the surface where pairing occurs. In other words, only a partial, not complete, gap is opened.

When $\lambda_0 > \max\{\lambda_2^*(0), 2\sqrt{W^2 + \lambda_\pi^2} - |\lambda_\pi| - W\}$ and at quarter-filling, all $\boldsymbol{k}$ blocks are singly occupied. The zero-energy surface is absent, hence the low-energy excitations of electrons, pairs, or quartets do not exist. However, this state is not an insulating state because of the presence of low-energy particle-hole excitations. In a $\boldsymbol{k}$ block with $t_{\boldsymbol{k}} \sim 0$, the state $\hat{c}^\dagger_{\uparrow,\boldsymbol{k}}|\Omega\rangle$ (or $\hat{c}^\dagger_{\downarrow,-\boldsymbol{k}}|\Omega\rangle$) can jump to $\hat{c}^\dagger_{\uparrow,\boldsymbol{\pi}+\boldsymbol{k}}|\Omega\rangle$ (or $\hat{c}^\dagger_{\downarrow,\boldsymbol{\pi}-\boldsymbol{k}}|\Omega\rangle$) with little energy, which corresponds to the particle-hole excitations. Therefore, we consider this state to be in the Luttinger liquid phase.

When $\lambda_0 > \lambda_1^*(0)$ and at half-filling, all $\boldsymbol{k}$ blocks are doubly occupied. The state is expressed as:

$$|\Psi\rangle = \prod_{\boldsymbol{k}} \hat{d}^\dagger_{\boldsymbol{k}} |\Omega\rangle. \tag{16}$$

Although the zero-energy surface is absent, the system exhibits low-energy excitations of other types. In a single $\boldsymbol{k}$ block, there are six states with an occupancy of two (see Table I), comprising three singlets and one triplet. Their eigenvalues are

$$\begin{aligned} E_{2,0,-} &= -4\lambda_0 + 2\lambda_\pi - 2\sqrt{t_{\boldsymbol{k}}^2 + \lambda_\pi^2} - 2\mu, \\ E_{2,0,+} &= -4\lambda_0 + 2\lambda_\pi + 2\sqrt{t_{\boldsymbol{k}}^2 + \lambda_\pi^2} - 2\mu, \\ E_{2,\pi,\mathrm{s}} &= -4\lambda_0 + 4\lambda_\pi - 2\mu, \\ E_{2,\pi,\mathrm{t}} &= -4\lambda_0 - 2\mu. \end{aligned} \tag{17}$$

For nonzero $t_{\boldsymbol{k}}$, $E_{2,0,-}$ is always the smallest, and the second smallest is $E_{2,\pi,\mathrm{s}}$ if $\lambda_\pi < 0$, or $E_{2,\pi,\mathrm{t}}$ if $\lambda_\pi > 0$. Namely, in a $\boldsymbol{k}$ block with $t_{\boldsymbol{k}} \sim 0$, the ground state $\hat{d}^\dagger_{\boldsymbol{k}}|\Omega\rangle$ can jump to the first excited state with little energy, which is the triplet state (corresponding to $E_{2,\pi,\mathrm{t}}$) or the singlet state (corresponding to $E_{2,\pi,\mathrm{s}}$). Therefore, we also consider this state to be in the Luttinger liquid phase. In the Appendix, we will introduce various possible ground states and explore the possible phase evolutions with varying charge fillings under different parameter conditions.

## IV. SUMMARY AND OUTLOOK

To sum up, we investigated the two-site cluster extension of the HK model. We found that the ground state exhibits a diverse array of phases, including the charge-4$e$ phase, the charge-2$e$ phase, the half-filled and quarter-filled Luttinger liquid phase, the metallic phase, and the pseudogap phase. These discoveries involve charge-4$e$ superconductivity and Luttinger liquid behavior, advancing our understanding of strongly correlated physics.

Drawing from previous research relevant to the HK model, we can summarize its fundamental spirit—constructing exactly solvable lattice models by utilizing simple $\boldsymbol{k}$ blocks. Further considerations can be made for simple interactions between these blocks, such as density-density interaction [61], spin-spin interaction [62], rendering them equivalent to some simpler models. Alternatively, one can consider coupling with order parameters [28,36], making them equivalent to

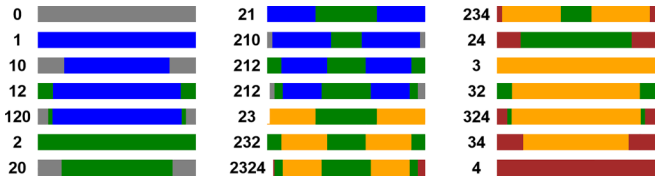


FIG. 3. Occupation numbers in $\boldsymbol{k}$ blocks in various types of ground states.

Ginzburg-Landau models. Likewise, our work represents a significant extension of the HK model, expanding the $k$ block from one site to two sites. Following this approach, it can be further expanded to clusters with four sites, six sites, and possibly more, bringing about richer physics.

## APPENDIX A: VARIOUS TYPES OF GROUND STATES

Based on the occupation numbers within $\boldsymbol{k}$ blocks, the ground states of the lattice model can be categorized into 21 types. We use the colored bars to illustrate these types, as shown in Fig. 3. The center of the bar represents the $\boldsymbol{k} = 0$ block, while the two ends correspond to the blocks with $\boldsymbol{k}$ at the boundary of the half of the first Brillouin zone. We also use a series of numbers to indicate the type of state; its meaning is self-evident and will be further elaborated in the description below. Owing to the particle-hole symmetry, we only need to consider states with fillings not larger than a half, which amounts to 11 types. For convenience, we use $k$ to replace $\boldsymbol{k}$ below, and stipulate the norm of $k$ such that $|k| < |k'|$ implies $t_k > t_{k'}$.

(i) Type 0. The vacuum state $|\Omega\rangle$ signifies that all $k$ blocks are empty and is labeled as type 0, and it is in a trivial insulating phase.

(ii) Type 1. The state of type 1 signifies that all $k$ blocks are singly occupied and it is in a Luttinger liquid phase. A typical state of this type is given by

$$\prod_{k} \hat{c}^{\dagger}_{\uparrow,k}|\Omega\rangle, \tag{A1}$$

noting that arbitrary $\hat{c}^{\dagger}_{\uparrow,k}$'s can be replaced by $\hat{c}^{\dagger}_{\downarrow,-k}$'s.

(iii) Type 10. A typical state of type 10 can be described as

$$\prod_{|k|<k_{1,0}} \hat{c}^{\dagger}_{\uparrow,k}|\Omega\rangle. \tag{A2}$$

In this state, the blocks with $|k| < k_{1,0}$ are singly occupied, and the blocks with $|k| \geqslant k_{1,0}$ are empty. This state is in the metallic phase.

(iv) Type 12. A typical state of type 12 can be described as

$$\prod_{|k|<k_{1,2}} \hat{c}^{\dagger}_{\uparrow,k} \prod_{|k|\geqslant k_{1,2}} \hat{d}^{\dagger}_{k}|\Omega\rangle. \tag{A3}$$

In this state, the blocks with $|k| < k_{1,2}$ are singly occupied, and other blocks are doubly occupied. This state is in the metallic phase.

(v) Type 120. A typical state of type 120 can be described as

$$\prod_{|k|<k_{1,2}} \hat{c}^{\dagger}_{\uparrow,k} \prod_{k_{1,2}\leqslant|k|<k_{2,0}} \hat{d}^{\dagger}_{k}|\Omega\rangle. \tag{A4}$$

In this state, the blocks with $|k| < k_{1,2}$ are singly occupied, the blocks with $k_{1,2} \leqslant |k| < k_{2,0}$ are doubly occupied, and other blocks are empty. This state is in the pseudogap phase, for the coexistence of electrons (at $|k| = k_{1,2}$) and pairs (at $|k| = k_{2,0}$) at zero energy.

(vi) Type 2. The state of type 2 signifies that all $k$ blocks are doubly occupied, described as

$$\prod_{k} \hat{d}^{\dagger}_{k}|\Omega\rangle. \tag{A5}$$

This state is commonly in the Luttinger liquid phase.

(vii) Type 20. The state of type 20 is described as

$$\prod_{|k|<k_{2,0}} \hat{d}^{\dagger}_{k}|\Omega\rangle. \tag{A6}$$

In this state, the blocks with $|k| < k_{2,0}$ are doubly occupied, and other blocks are empty. This state is commonly in the charge-$2e$ phase.

(viii) Type 21. A typical state of type 21 is described as

$$\prod_{|k|<k_{2,1}} \hat{d}^{\dagger}_{k} \prod_{|k|\geqslant k_{2,1}} \hat{c}^{\dagger}_{\uparrow,k}|\Omega\rangle. \tag{A7}$$

In this state, the blocks with $|k| < k_{2,1}$ are doubly occupied, and other blocks are singly occupied. This state is in the metallic phase.

(ix) Type 210. A typical state of type 210 is described as

$$\prod_{|k|<k_{2,1}} \hat{d}^{\dagger}_{k} \prod_{k_{2,1}\leqslant|k|<k_{1,0}} \hat{c}^{\dagger}_{\uparrow,k}|\Omega\rangle. \tag{A8}$$

In this state, the blocks with $|k| < k_{2,1}$ are doubly occupied, the blocks with $k_{2,1} \leqslant |k| < k_{1,0}$ are singly occupied, and other blocks are singly occupied. This state is in the metallic phase.

(x) Type 212. A typical state of type 212 is described as

$$\prod_{|k|<k_{2,1}} \hat{d}^{\dagger}_{k} \prod_{k_{2,1}\leqslant|k|<k_{1,2}} \hat{c}^{\dagger}_{\uparrow,k} \prod_{|k|\geqslant k_{1,2}} \hat{d}^{\dagger}_{k}|\Omega\rangle. \tag{A9}$$

In this state, the blocks with $|k| < k_{2,1}$ or $|k| \geqslant k_{1,2}$ are doubly occupied, and the blocks with $k_{2,1} \leqslant |k| < k_{1,2}$ are singly occupied. This state is in the metallic phase.

(xi) Type 2120. A typical state of type 2120 is described as

$$\prod_{|k|<k_{2,1}} \hat{d}^{\dagger}_{k} \prod_{k_{2,1}\leqslant|k|<k_{1,2}} \hat{c}^{\dagger}_{\uparrow,k} \prod_{k_{1,2}\leqslant|k|<k_{2,0}} \hat{d}^{\dagger}_{k}|\Omega\rangle. \tag{A10}$$

In this state, the blocks with $|k| < k_{2,1}$ or $k_{1,2} \leqslant |k| < 0$ are doubly occupied, the blocks with $k_{2,1} \leqslant |k| < k_{1,2}$ are singly occupied, and other blocks are empty. This state is in the pseudogap phase, for the coexistence of electrons (at $|k| = k_{2,1}$ and $|k| = k_{1,2}$) and pairs (at $|k| = k_{2,0}$) at zero energy.

**Summary**

Let us summarize the 11 types of ground states presented above. Among them, except for the vacuum (0), two are in the Luttinger liquid phase (1, 2), one is in the charge-$2e$ phase (20), two are in the pseudogap phase (120, 120), and the remaining five are in the metallic phase (10, 12, 21, 210, 212).

In addition to the 11 types, there are two other possible types of ground states. In the scenario where $\mu = 0$ and $\lambda_0 < \lambda_1^*(0)$, the minimal units in some or all $k$ blocks are quartets. The energies of these quartets are all zero, so their presence or

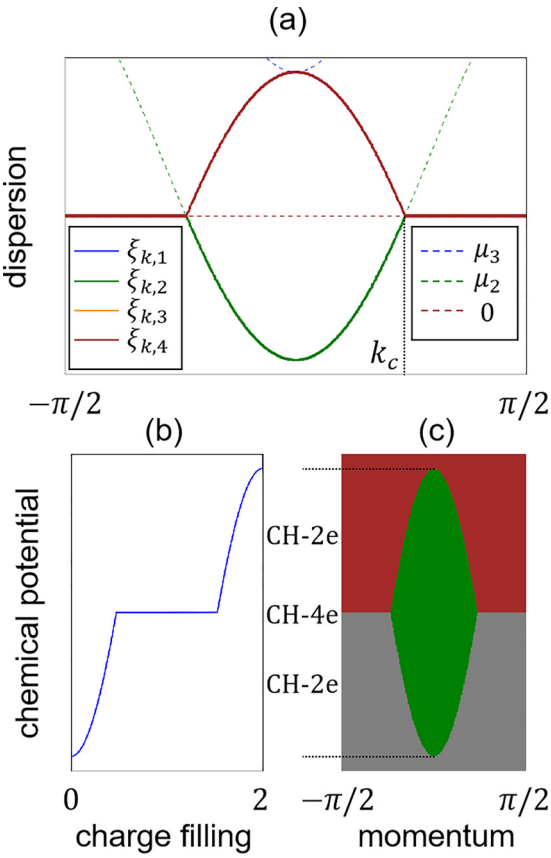


FIG. 4. Case (ii): Phase transition at a typical set of parameters, $\lambda_0/W = -0.15$ and $\lambda_\pi/W = 0.75$, on 1D lattice with 1024 sites. $t_k = W\cos k$ is assumed. In (a), the solid lines represent for $\xi_{k,1}$ (blue, not shown), $\xi_{k,2}$ (green), $\xi_{k,3}$ (orange, not shown), and $\xi_{k,4}$ (brown). The dashed lines represent for $\mu_3(t_k)$ (blue), $\mu_2(t_k)$ (green), and 0 (brown). (b) shows the variation of charge density with chemical potential. (c) shows the change in the occupation numbers of $k$ blocks with respect to the chemical potential.

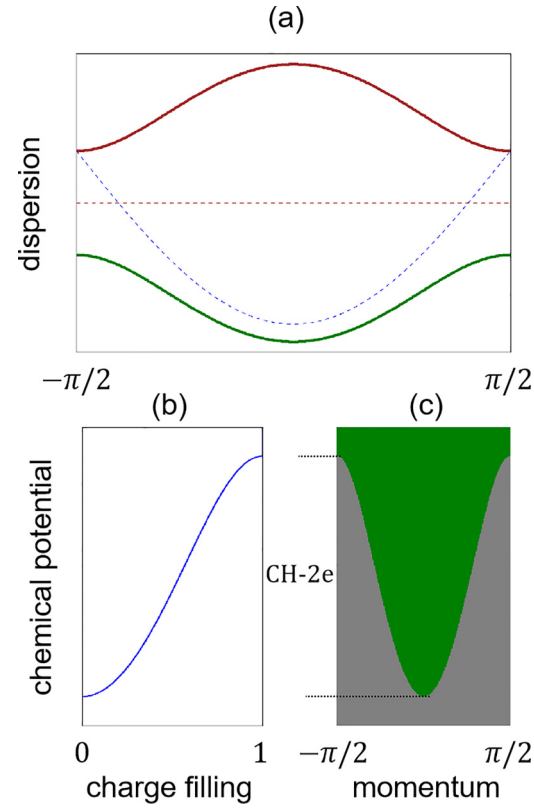


FIG. 5. Case (iii): $\lambda_0/W = 0.15$, $\lambda_\pi/W = 0.75$.

absence does not affect the ground-state energy. We call this state as being in the charge-4$e$ phase.

## APPENDIX B: EVOLUTIONS OF PHASES

In this part, we will demonstrate several types of transitions of ground states with varying $\mu$'s at given parameters $\lambda_0$, $\lambda_\pi$, and $W$. Here, we specify some important critical values. For $\lambda_0$, the values of $\lambda_1^*(W)$, $\lambda_1^*(0)$, $\lambda_2^*(W)$, and $\lambda_2^*(0)$ mark the boundaries between different distributions of minimal units in $k$ blocks. For $|\lambda_\pi|$, the comparison with $3W/4$ determines whether $\mu_1(t_k)$'s minimum value is $\mu_1(0)$ or $\mu_1(W)$, and the comparison with $\sqrt{3}W$ determines whether $\mu_1(t_k)$'s maximum value is $\mu_1(|\lambda_\pi|/\sqrt{3})$ or $\mu_1(W)$.

(i) When $\lambda_0 < \lambda_1^*(W)$. In this scenario, the minimal units in all $k$ blocks are quartets. The effective dispersion relation becomes $\xi_{k,i} = -\mu$ for all $k$ and $i$. When $\mu < 0$, all $k$ blocks are empty, whereas when $\mu > 0$, all $k$ blocks are fully occupied. When $\mu = 0$, the system will be in a charge-4$e$ phase.

(ii) When $\lambda_1^*(W) < \lambda_0 < \lambda_1^*(0)$. Let $\lambda_0 = \lambda_1^*(t_{k_c})$. In this scenario, the minimal units in blocks with $|k| < k_c$ are pairs, and those in blocks with $|k| > k_c$ are quartets. Figure 4 displays the effective dispersion [Fig. 4(a), setting $\mu = 0$], the variation of charge density with chemical potential [Fig. 4(b)], and the change in the occupation numbers of $k$ blocks with respect to the chemical potential [Fig. 4(c)], for a typical set of parameters on 1D lattice with 1024 sites. As the charge density varies from 0–2, the ground state undergoes a transition from the vacuum state (0) to the charge-2$e$ phase (20), to the charge-4$e$ phase at $\mu = 0$, to the charge-2$e$ phase (24), and finally to the fully occupied state (4).

(iii) When $\lambda_1^*(0) < \lambda_0 < \lambda_2^*(W)$. In this scenario, the minimal units in all $k$ blocks are pairs. The effective dispersion is simply $\xi_{k,1} = \xi_{k,2} = \mu_2(t_k) - \mu$ and $\xi_{k,3} = \xi_{k,4} = -\mu_2(t_k) - \mu$. Figure 5 displays the effective dispersion [Fig. 5(a)], the variation of charge density [Fig. 5(b)], and the change in the occupation numbers of $k$ blocks [Fig. 5(c)]. As the charge density varies from 0–1, the ground state undergoes a transition from the vacuum state (0), to the charge-2$e$ phase (20), and to the half-filled Luttinger liquid phase (2).

(iv) When $\lambda_2^*(W) < \lambda_0 < |\lambda_\pi|/\sqrt{3}$ and $|\lambda_\pi| < \sqrt{3}W$. Let $\lambda_0 = \lambda_2^*(t_{k_c})$ and we can find $t_{k_c} > |\lambda_\pi|/\sqrt{3}$. In this scenario, the minimal units in blocks with $|k| < k_c$ are electrons, and those in blocks with $|k| < k_c$ are pairs. Note that $\mu_1(t)$ is monotonically decreasing in the interval $[t_{k_c}, W]$, and that $\mu_1(t_{k_c}) = \mu_2(t_{k_c})$. Figure 6 displays the effective dispersion [Fig. 6(a)], the variation of charge density [Fig. 6(b)], and the change in the occupation numbers of $k$ blocks [Fig. 6(c)]. As the charge density varies from 0–1, the ground state undergoes a transition from the vacuum state (0), to the metallic phase (10, 210), to the charge-2$e$ phase (20), and to the half-filled Luttinger liquid phase (2).

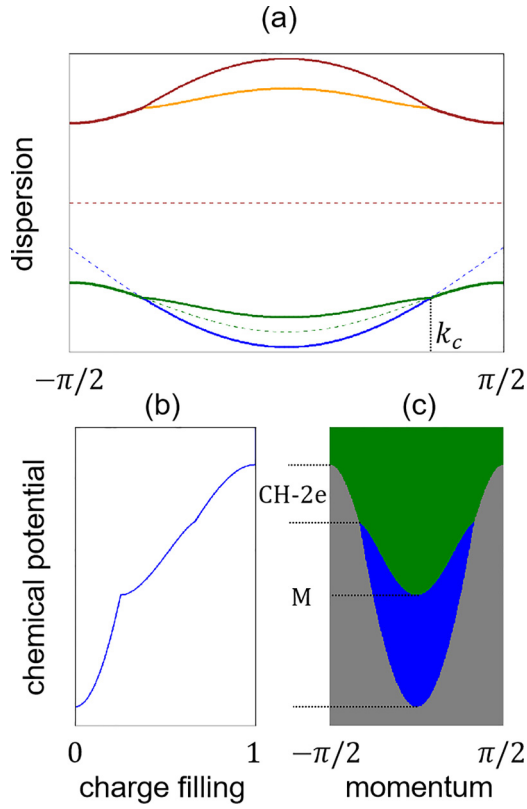


FIG. 6. Case (iv): $\lambda_0/W = 0.4$, $\lambda_\pi/W = 0.75$.

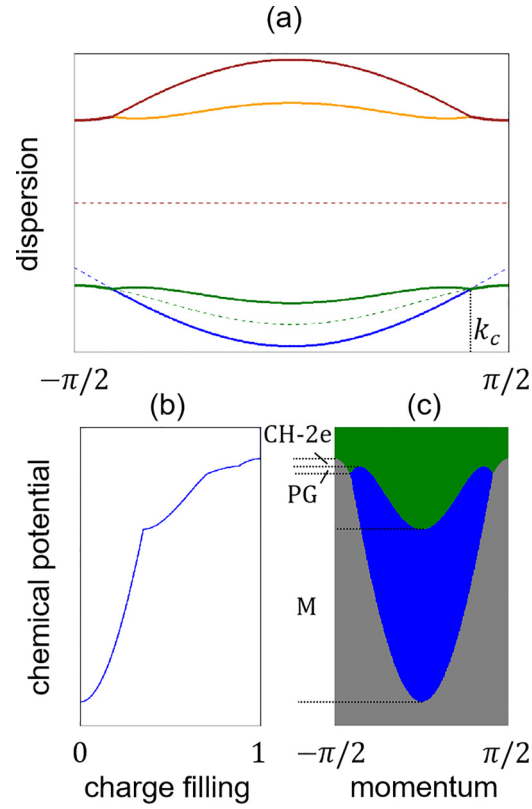


FIG. 7. Case (v): $\lambda_0/W = 0.525$, $\lambda_\pi/W = 0.75$.

(v) When $\frac{|\lambda_\pi|}{\sqrt{3}} < \lambda_0 < (\sqrt{3}-1)|\lambda_\pi|$ and $|\lambda_\pi| < \sqrt{3}W$. Let $\lambda_0 = \lambda_2^*(t_{k_c})$ and we can find $t_{k_c} < |\lambda_\pi|/\sqrt{3}$. In this scenario, the minimal units in blocks with $|k| < k_c$ are electrons, and those in blocks with $|k| < k_c$ are pairs. Note that $\mu_1(t)$ is monotonically decreasing in the interval $[|\lambda_\pi|/\sqrt{3}, W]$ and increasing in the interval $[t_{k_c}, |\lambda_\pi|/\sqrt{3}]$. Note that $\mu_1(|\lambda_\pi|/\sqrt{3}) < \mu_2(0)$. Figure 7 displays the effective dispersion [Fig. 7(a)], the variation of charge density [Fig. 7(b)], and the change in the occupation numbers of $k$ blocks [Fig. 7(c)]. If $\mu_1(W) < \mu_1(t_{k_c})$, as the charge density varies from 0–1, the ground state undergoes a transition from the vacuum state (0), to the metallic phase (10, 210), to the pseudogap phase (2120), to the charge-2$e$ phase (20), and to the half-filled Luttinger liquid phase (2). If $\mu_1(W) > \mu_1(t_{k_c})$, the ground state undergoes a transition from the vacuum state (0) to the metallic phase (10), to the pseudogap phase (120, 2120), to the charge-2$e$ phase (20), and to the half-filled Luttinger liquid phase (2).

(vi) When $(\sqrt{3}-1)|\lambda_\pi| < \lambda_0 < |\lambda_\pi|$ and $|\lambda_\pi| < 3W/4$. Let $\lambda_0 = \lambda_2^*(t_{k_c})$. In this scenario, the minimal units in blocks with $|k| < k_c$ are electrons, and those in blocks with $|k| < k_c$ are pairs. Note that $\mu_1(t)$ is monotonically decreasing in the interval $[|\lambda_\pi|/\sqrt{3}, W]$ and increasing in the interval $[t_{k_c}, |\lambda_\pi|/\sqrt{3}]$. Note that $\mu_1(W) < \mu_2(0) < \mu_1(|\lambda_\pi|/\sqrt{3})$, and $\mu_1(W) < \mu_1(0) < \mu_1(t_{k_c})$. Figure 8 displays the effective dispersion [Fig. 8(a)], the variation of charge density [Fig. 8(b)], and the change in the occupation numbers of $k$ blocks [Fig. 8(c)]. As the charge density varies from 0–1, the ground state undergoes a transition from the vacuum state (0)

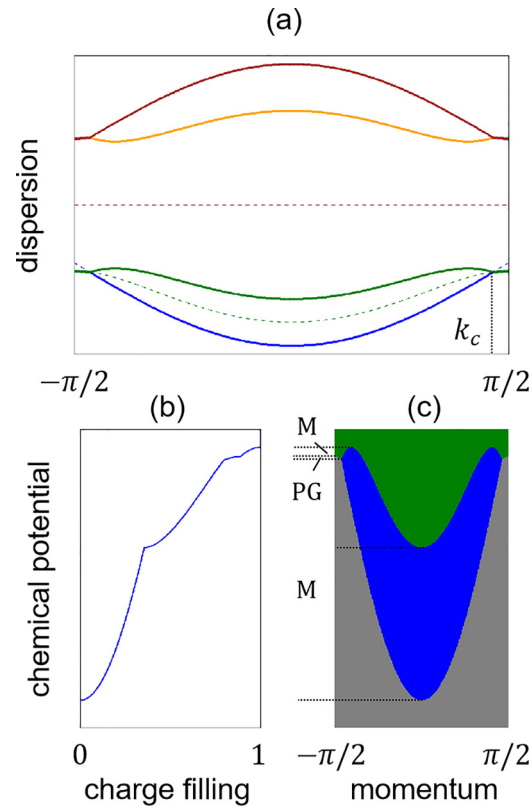


FIG. 8. Case (vi): $\lambda_0/W = 0.4$, $\lambda_\pi/W = 0.5$.

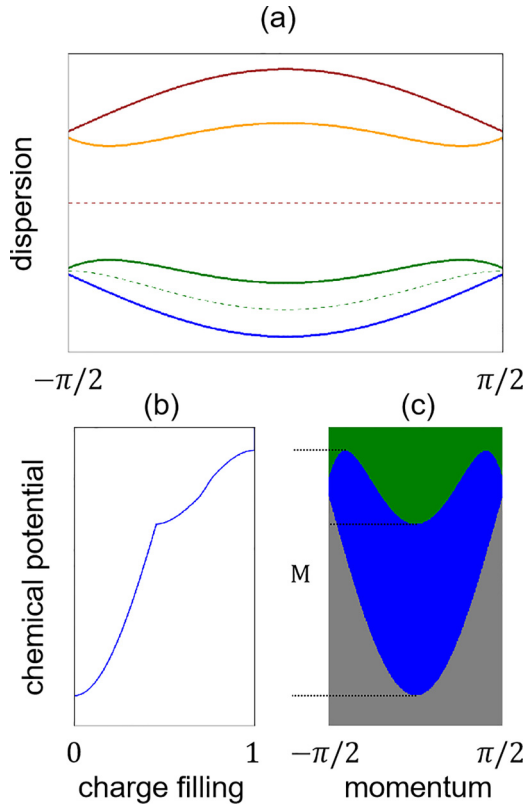


FIG. 9. Case (vii): $\lambda_0/W = 0.55$, $\lambda_\pi/W = 0.5$.

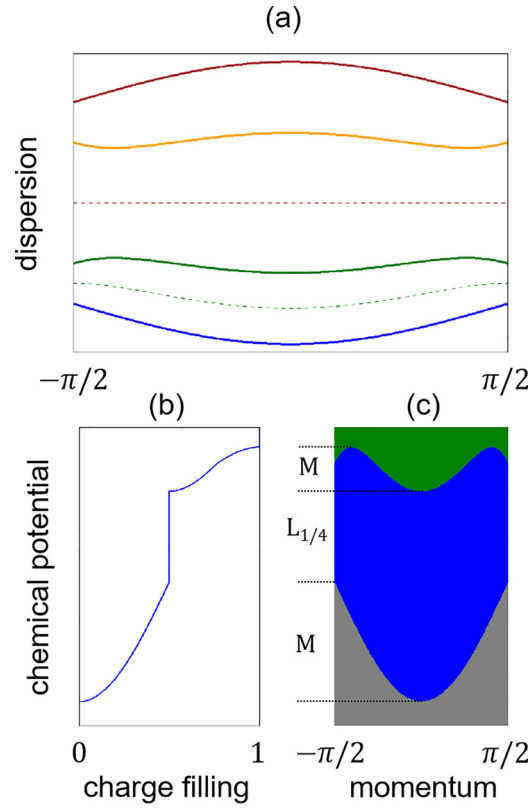


FIG. 10. Case (viii): $\lambda_0/W = 1.0$, $\lambda_\pi/W = 0.5$.

to the metallic phase (10, 210), to the pseudogap phase (2120), to the metallic phase (212), and to the half-filled Luttinger liquid phase (2).

(vii) When $|\lambda_\pi| < \lambda_0 < \sqrt{W^2 + \lambda_\pi^2} - W/2$ and $|\lambda_\pi| < 3W/4$. In this scenario, the minimal units in all $k$ blocks are electrons, and thus $\xi_{k,1} = \mu_3(t_k) - \mu$ and $\xi_{k,2} = \mu_1(t_k) - \mu$. Note that $\mu_1(W) < \mu_3(0) < \mu_1(0)$. Figure 9 displays the effective dispersion [Fig. 9(a)], the variation of charge density [Fig. 9(b)], and the change in the occupation numbers of $k$ blocks [Fig. 9(c)]. As the charge density varies from 0–1, the ground state undergoes a transition from the vacuum state (0) to the metallic phase (10, 210, 21, 212), and to the half-filled Luttinger liquid phase (2).

(viii) When $\lambda_0 > \sqrt{W^2 + \lambda_\pi^2} - W/2$ and $|\lambda_\pi| < 3W/4$. In this scenario, the minimal units in all $k$ blocks are electrons, and thus $\xi_{k,1} = \mu_3(t_k) - \mu$ and $\xi_{k,2} = \mu_1(t_k) - \mu$. Note that $\mu_3(0) < \mu_1(W) < \mu_1(0)$. Figure 10 displays the effective dispersion [Fig. 10(a)], the variation of charge density [Fig. 10(b)], and the change in the occupation numbers of $k$ blocks [Fig. 10(c)]. As the charge density varies from 0–1, the ground state undergoes a transition from the vacuum state (0) to the metallic phase (10), to the quarter-filled Luttinger liquid phase (1), to the metallic phase (21, 212), and to the half-filled Luttinger liquid phase (2).

(ix) When $(\sqrt{3} - 1)|\lambda_\pi| < \lambda_0 < 2\sqrt{W^2 + \lambda_\pi^2} - W - |\lambda_\pi|$ and $3W/4 < |\lambda_\pi| < \sqrt{3}W$. Let $\lambda_0 = \lambda_2^*(t_{k_c})$. In this scenario, the minimal units in blocks with $|k| < k_c$ are electrons, and those in blocks with $|k| < k_c$ are pairs. Note that $\mu_1(W) < \mu_2(0) < \mu_1(|\lambda_\pi|/\sqrt{3})$. Figure 11 displays the effective dispersion [Fig. 11(a)], the variation of charge density

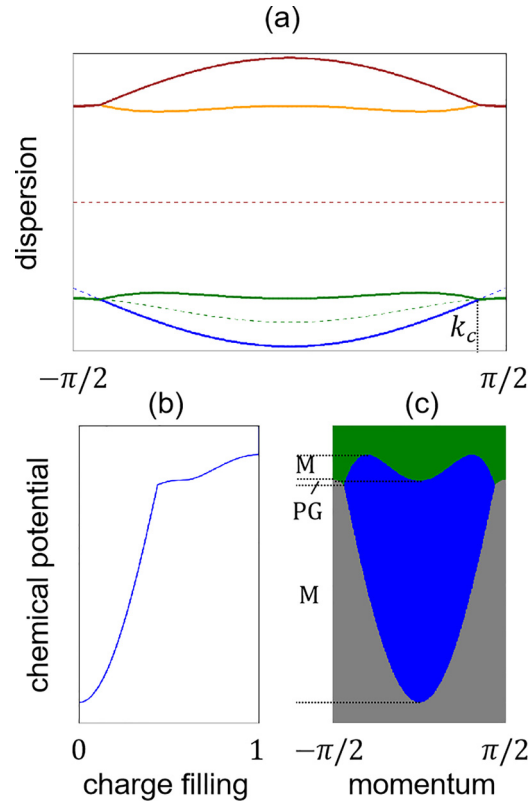


FIG. 11. Case (ix): $\lambda_0/W = 0.825$, $\lambda_\pi/W = 1.0$.

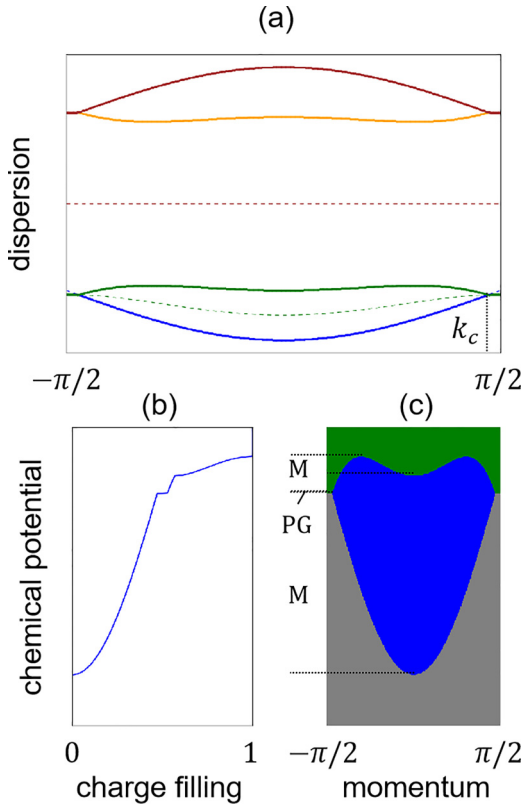


FIG. 12. Case (x): $\lambda_0/W = 0.915$, $\lambda_\pi/W = 1.0$.

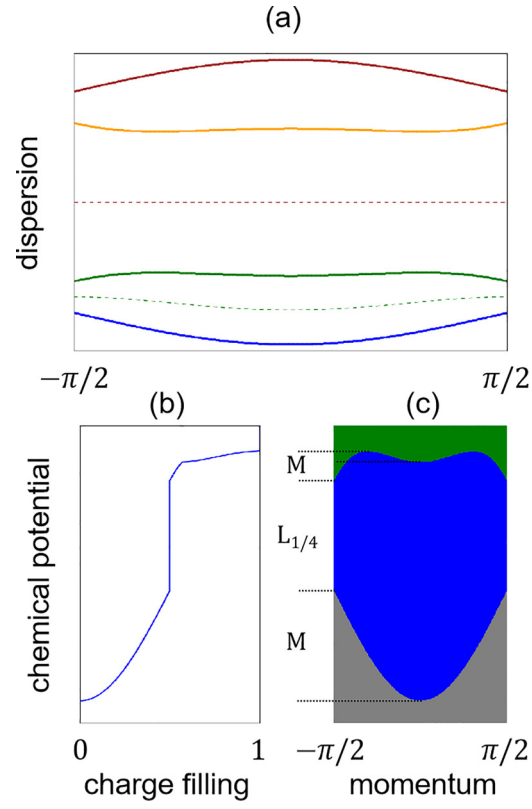


FIG. 13. Case (xi): $\lambda_0/W = 1.5$, $\lambda_\pi/W = 1.0$.

[Fig. 11(b)], and the change in the occupation numbers of $k$ blocks [Fig. 11(c)]. If $\mu_1(W) > \mu_1(t_{k_c})$, as the charge density varies from 0–1, the ground state undergoes a transition from the vacuum state (0) to the metallic phase (10), to the pseudogap phase (120, 2120), to the metallic phase (212), and to the half-filled Luttinger liquid phase (2). If $\mu_1(W) < \mu_1(t_{k_c})$, as the charge density varies from 0–1, the ground state undergoes a transition from the vacuum state (0), to the metallic phase (10, 210), to the pseudogap phase (2120), to the metallic phase (212), and to the half-filled Luttinger liquid phase (2).

(x) When $2\sqrt{W^2+\lambda_\pi^2} - W - |\lambda_\pi| < \lambda_0 < |\lambda_\pi|$ and $3W/4 < |\lambda_\pi| < \sqrt{3}W$. Let $\lambda_0 = \lambda_2^*(k_c)$. In this scenario, the minimal units in blocks with $|k| < k_c$ are electrons, and those in blocks with $|k| > k_c$ are pairs. Note that $\mu_2(0) < \mu_1(W)$. Figure 12 displays the effective dispersion [Fig. 12(a)], the variation of charge density [Fig. 12(b)], and the change in the occupation numbers of $k$ blocks [Fig. 12(c)]. As the charge density varies from 0–1, the ground state undergoes a transition from the vacuum state (0) to the metallic phase (10), to the pseudogap phase (120), to the metallic phase (12, 212) and to the half-filled Luttinger liquid phase (2).

(xi) When $\lambda_0 > |\lambda_\pi|$ and $3W/4 < |\lambda_\pi| < \sqrt{3}W$. In this scenario, the minimal units in all $k$ blocks are electrons, and thus $\xi_{k,1} = \mu_3(t_k) - \mu$ and $\xi_{k,2} = \mu_1(t_k) - \mu$. Note that $\mu_1(0) < \mu_3(0)$. Figure 13 displays the effective dispersion [Fig. 13(a)], the variation of charge density [Fig. 13(b)], and the change in the occupation numbers of $k$ blocks [Fig. 13(c)]. As the charge density varies from 0–1, the ground state undergoes a transition from the vacuum state (0) to the metallic phase (10), to the quarter-filled Luttinger liquid phase (1), to

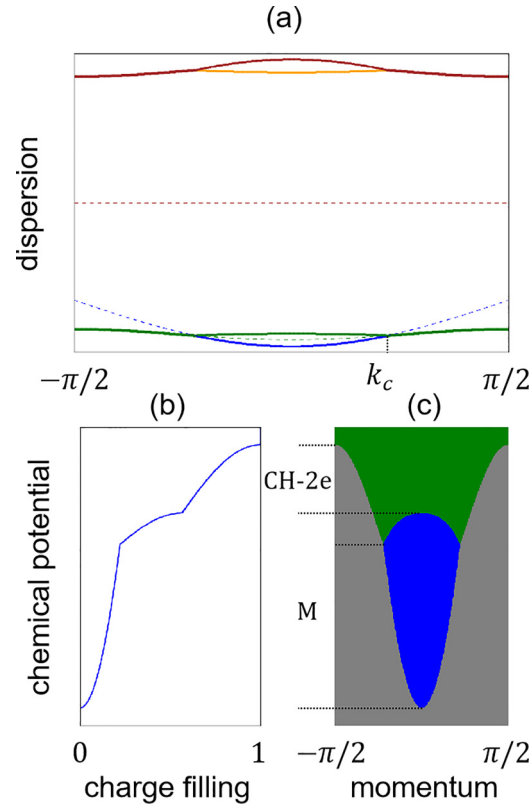


FIG. 14. Case (xii): $\lambda_0/W = 1.375$, $\lambda_\pi/W = 2.0$.

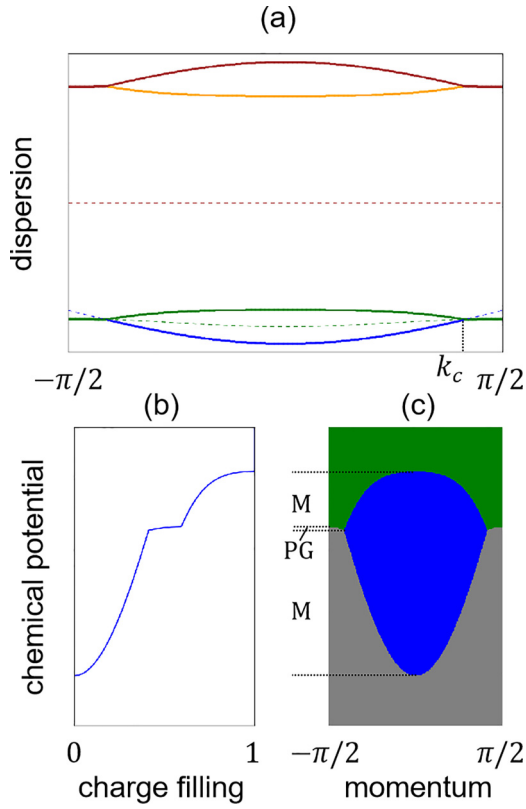


FIG. 15. Case (xiii): $\lambda_0/W = 1.75$, $\lambda_\pi/W = 2.0$.

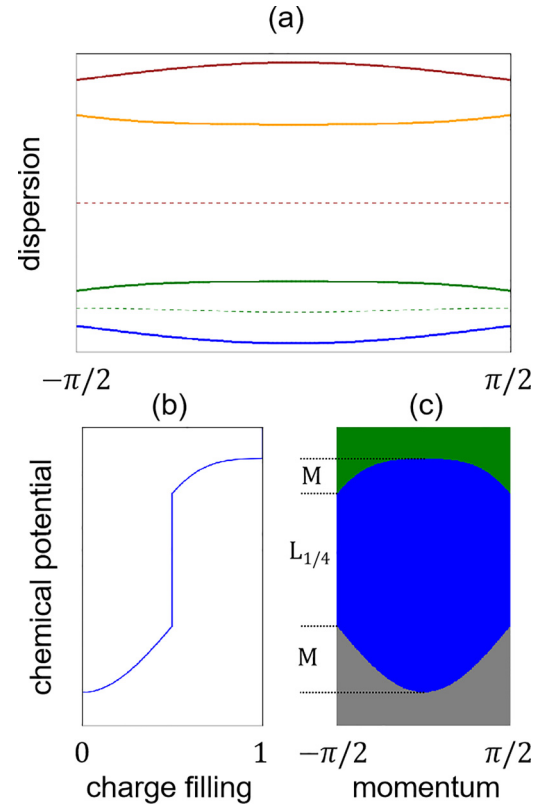


FIG. 16. Case xiv: $\lambda_0/W = 3.0$, $\lambda_\pi/W = 2.0$.

the metallic phase (12, 212), and to the half-filled Luttinger liquid phase (2).

(xii) When $\lambda_2^*(W) < \lambda_0 < 2\sqrt{W^2+\lambda_\pi^2} - W - |\lambda_\pi|$ and $|\lambda_\pi| > \sqrt{3}W$. Let $\lambda_0 = \lambda_2^*(t_{k_c})$. In this scenario, the minimal units in blocks with $|k| < k_c$ are electrons and those in blocks with $|k| > k_c$ are pairs. Note that $\mu_1(W) < \mu_2(0)$. Figure 14 displays the effective dispersion [Fig. 14(a)], the variation of charge density [Fig. 14(b)], and the change in the occupation numbers of $k$ blocks [Fig. 14(c)]. As the charge density varies from 0–1, the ground state undergoes a transition from the vacuum state (0) to the metallic phase (10), to the pseudogap phase (120), to the charge-2$e$ phase (20), and to the half-filled Luttinger liquid phase (2).

(xiii) When $2\sqrt{W^2+\lambda_\pi^2} - W - |\lambda_\pi| < \lambda_0 < |\lambda_\pi|$ and $|\lambda_\pi| > \sqrt{3}W$. Let $\lambda_0 = \lambda_2^*(t_{k_c})$. In this scenario, the minimal units in blocks with $|k| < k_c$ are electrons and those in blocks with $|k| > k_c$ are pairs. Note that $\mu_1(W) > \mu_2(0)$. Figure 15 displays the effective dispersion [Fig. 15(a)], the variation of charge density [Fig. 15(b)], and the change in the occupation numbers of $k$ blocks [Fig. 15(c)]. As the charge density varies from 0–1, the ground state undergoes a transition from the vacuum state (0) to the metallic phase (10), to the pseudogap phase (120), to the metallic phase (12), and to the half-filled Luttinger liquid phase (2).

(xiv) When $\lambda_0 > |\lambda_\pi|$ and $|\lambda_\pi| > \sqrt{3}W$. In this scenario, the minimal units in all $k$ blocks are electrons. Figure 16 displays the effective dispersion [Fig. 16(a)], the variation of charge density [Fig. 16(b)], and the change in the occupation numbers of $k$ blocks [Fig. 16(c)]. As the charge density varies from 0–1, the ground state undergoes a transition from the vacuum state (0) to the metallic phase (10), to the quarter-filled Luttinger liquid phase (1), to the metallic phase (12), and to the half-filled Luttinger liquid phase (2).

**Summary**

The text above displays transitions of the ground state with charge filling under 14 different parameter conditions.

[1] N. F. Mott, Metal-insulator transition, Rev. Mod. Phys. **40**, 677 (1968).

[2] M. Imada, A. Fujimori, and Y. Tokura, Metal-insulator transitions, Rev. Mod. Phys. **70**, 1039 (1998).

[3] O. Gunnarsson, M. Calandra, and J. E. Han, Colloquium: Saturation of electrical resistivity, Rev. Mod. Phys. **75**, 1085 (2003).

[4] Chandra M. Varma, Colloquium: Linear in temperature resistivity and associated mysteries including high temperature superconductivity, Rev. Mod. Phys. **92**, 031001 (2020).

[5] V. R. Shaginyan, A. Z. Msezane and G. S. Japaridze, Peculiar physics of heavy-fermion metals: Theory versus experiment, Atoms **10**, 67 (2022).

[6] P. W. Phillips, N. E. Hussey, and P. Abbamonte, Stranger than metals, Science **377**, eabh4273 (2022).

[7] J. G. Bednorz and K. A. Müller, Possible high $T_c$ superconductivity in the Ba-La-Cu-O system, Z. Phys. B **64**, 189 (1986).

[8] P. A. Lee, N. Nagaosa, and X.-G. Wen, Doping a Mott insulator: Physics of high-temperature superconductivity, Rev. Mod. Phys. **78**, 17 (2006).

[9] J. A. Sobota, Y. He, and Z.-X. Shen, Angle-resolved photoemission studies of quantum materials, Rev. Mod. Phys. **93**, 025006 (2021).

[10] P. W. Anderson, The resonating valence bond state in $La_2CuO_4$ and superconductivity, Science **235**, 1196 (1987).

[11] N. E. Bickers, D. J. Scalapino, and S. R. White, Conserving approximations for strongly correlated electron systems: Bethe-Salpeter equation and dynamics for the two-dimensional Hubbard model, Phys. Rev. Lett. **62**, 961 (1989).

[12] D. J. Scalapino, A common thread: The pairing interaction for unconventional superconductors, Rev. Mod. Phys. **84**, 1383 (2012).

[13] R. Micnas, J. Ranninger, and S. Robaszkiewicz, Superconductivity in narrow-band systems with local nonretarded attractive interactions, Rev. Mod. Phys. **62**, 113 (1990).

[14] H. Kontani, Anomalous transport phenomena in Fermi liquids with strong magnetic fluctuations, Rep. Prog. Phys. **71**, 026501 (2008).

[15] E. W. Huang, R. Sheppard, B. Moritz and T. P. Devereaux, Strange metallicity in the doped Hubbard model, Science **366**, 987 (2019).

[16] R. Blankenbecler, D. J. Scalapino, and R. L. Sugar, Monte Carlo calculations of coupled boson-fermion systems. I, Phys. Rev. D **24**, 2278 (1981).

[17] C.-C. Chang, S. Gogolenko, J. Perez, Z. Bai and R. T. Scalettar, Recent advances in determinant quantum Monte Carlo, Philos. Mag. **95**, 1260 (2015).

[18] Z.-X. Li and H. Yao, Sign-problem-free fermionic quantum Monte Carlo: Developments and applications, Annu. Rev. Condens. Matter Phys. **10**, 337 (2019).

[19] S. R. White, Density matrix formulation for quantum renormalization groups, Phys. Rev. Lett. **69**, 2863 (1992).

[20] U. Schollwöck, The density-matrix renormalization group, Rev. Mod. Phys. **77**, 259 (2005).

[21] F. Verstraete, T. Nishino, U. Schollwöck, M. C. Bañuls, G. K. Chan and M. E. Stoudenmire, Density matrix renormalization group, 30 years on, Nat. Rev. Phys. **5**, 273 (2023).

[22] J. Eisert, M. Cramer, and M. B. Plenio, Colloquium: Area laws for the entanglement entropy, Rev. Mod. Phys. **82**, 277 (2010).

[23] A. Georges and G. Kotliar, Hubbard model in infinite dimensions, Phys. Rev. B **45**, 6479 (1992).

[24] A. Georges, G. Kotliar, W. Krauth, and M. J. Rozenberg, Dynamical mean-field theory of strongly correlated fermion systems and the limit of infinite dimensions, Rev. Mod. Phys. **68**, 13 (1996).

[25] G. Rohringer, H. Hafermann, A. Toschi, A. A. Katanin, A. E. Antipov, M. I. Katsnelson, A. I. Lichtenstein, A. N. Rubtsov, and K. Held, Diagrammatic routes to nonlocal correlations beyond dynamical mean field theory, Rev. Mod. Phys. **90**, 025003 (2018).

[26] Y. Hatsugai and M. Kohmoto, Exactly solvable model of correlated lattice electrons in any dimensions, J. Phys. Soc. Jpn. **61**, 2056 (1992).

[27] L. Yeo and P. W. Phillips, Local entropies across the Mott transition in an exactly solvable model, Phys. Rev. D **99**, 094030 (2019).

[28] P. W. Phillips, L. Yeo, and E. W. Huang, Exact theory for superconductivity in a doped Mott insulator, Nat. Phys. **16**, 1175 (2020).

[29] J. Zaanen, Carriers that count, Nat. Phys. **16**, 1171 (2020).

[30] K. Yang, Exactly solvable model of Fermi arcs and pseudogap, Phys. Rev. B **103**, 024529 (2021).

[31] C. Setty, Superconductivity from Luttinger surfaces: Emergent Sachdev-Ye-Kitaev physics with infinite-body interactions, Phys. Rev. B **103**, 014501 (2021).

[32] P. W. Phillips, When the disorder is just right, Physics **14**, 88 (2021).

[33] H.-S. Zhu and Q. Han, Effects of electron correlation on superconductivity in the Hatsugai–Kohmoto model, Chin. Phys. B **30**, 107401 (2021).

[34] R. D. Nesselrodt and J. K. Freericks, Exact solution of two simple non-equilibrium electron-phonon and electron-electron coupled systems: The atomic limit of the Holstein-Hubbard model and the generalized Hatsugai-Komoto model, Phys. Rev. B **104**, 155104 (2021).

[35] J. Zhao, L. Yeo, E. W. Huang, and P. W. Phillips, Thermodynamics of an exactly solvable model for superconductivity in a doped Mott insulator, Phys. Rev. B **105**, 184509 (2022).

[36] Y. Li, V. Mishra, Y. Zhou, and F.-C. Zhang, Two-stage superconductivity in the Hatsugai–Kohomoto-BCS model, New J. Phys. **24**, 103109 (2022).

[37] Y. Zhong, Solvable periodic Anderson model with infinite-range Hatsugai-Kohmoto interaction: Ground-states and beyond, Phys. Rev. B **106**, 155119 (2022).

[38] P. Mai, B. E. Feldman, and P. W. Phillips, Topological Mott insulator at quarter filling in the interacting Haldane model, Phys. Rev. Res. **5**, 013162 (2023).

[39] M. M. Wysokiński and W. Brzezicki, Quantum anomalous Hall insulator in ionic Rashba lattice of correlated electrons, Phys. Rev. B **108**, 035121 (2023).

[40] J. Zhao, P. Mai, B. Bradlyn, and P. Phillips, Failure of topological invariants in strongly correlated matter, Phys. Rev. Lett. **131**, 106601 (2023).

[41] D. Manning-Coe and B. Bradlyn, Ground state stability, symmetry, and degeneracy in Mott insulators with long-range interactions, Phys. Rev. B **108**, 165136 (2023).

[42] J. Zhao, G. La Nave, and P. W. Phillips, Proof of a stable fixed point for strongly correlated electron matter, Phys. Rev. B **108**, 165135 (2023).

[43] R. Wang and K. Yang, Non-Fermi liquid behavior in a simple model of Fermi arcs and pseudogap, Mod. Phys. Lett. B **37**, 2350119 (2023).

[44] K. Jabłonowski, J. Skolimowski, W. Brzezicki, K. Byczuk, and M. M. Wysokiński, Topological Mott insulator in the odd-integer filled Anderson lattice model with Hatsugai-Kohmoto interactions, Phys. Rev. B **108**, 195145 (2023).

[45] W.-W. Yang, H.-G. Luo, and Y. Zhong, Bose metal in an exactly solvable model with infinite-range Hatsugai-Kohmoto interaction, Phys. Rev. B **108**, 235149 (2023).

[46] P. Mai, J. Zhao, B. E. Feldman, and P. W. Phillips, 1/4 is the new 1/2 when topology is intertwined with Mottness, Nat. Commun. **14**, 5999 (2023).

[47] M. Zhao, W.-W. Yang, H.-G. Luo, and Y. Zhong, Friedel oscillation in non-Fermi liquid: Lesson from exactly solvable Hatsugai–Kohmoto model, J. Phys.: Condens. Matter **35**, 495603 (2023).

[48] Y. Zhong, Notes on quantum oscillation for Hatsugai–Kohmoto model, Mod. Phys. Lett. B **38**, 2450027 (2024).
[49] S. A. Kivelson, V. J. Emery, and H. Q. Lin, Doped antiferromagnets in the weak-hopping limit, Phys. Rev. B **42**, 6523 (1990).
[50] E. Berg, E. Fradkin, S. A. Kivelson, and J. M. Tranquada, Striped superconductors: How spin, charge and superconducting orders intertwine in the cuprates, New J. Phys. **11**, 115004 (2009).
[51] E. Berg, E. Fradkin, and S. A. Kivelson, Charge-4*e* superconductivity from pair-density-wave order in certain high-temperature superconductors, Nat. Phys. **5**, 830 (2009).
[52] E. V. Herland, E. Babaev, and A. Sudbø, Phase transitions in a three dimensional $U(1) \times U(1)$ lattice London superconductor: Metallic superfluid and charge-4*e* superconducting states, Phys. Rev. B **82**, 134511 (2010).
[53] Y.-F. Jiang, Z.-X. Li, S. A. Kivelson, and H. Yao, Charge-4*e* superconductors: A Majorana quantum Monte Carlo study, Phys. Rev. B **95**, 241103(R) (2017).
[54] R. M. Fernandes and L. Fu, Charge-4*e* superconductivity from multicomponent nematic pairing: Application to twisted bilayer graphene, Phys. Rev. Lett. **127**, 047001 (2021).
[55] S.-K. Jian, Y. Huang, and H. Yao, Charge-4*e* superconductivity from nematic superconductors in two and three dimensions, Phys. Rev. Lett. **127**, 227001 (2021).
[56] N. V. Gnezdilov and Y. Wang, Solvable model for a charge-4*e* superconductor, Phys. Rev. B **106**, 094508 (2022).
[57] S. Zhou and Z. Wang, Chern Fermi pocket, topological pair density wave, and charge-4*e* and charge-6*e* superconductivity in kagomé superconductors, Nat. Commun. **13**, 7288 (2022).
[58] J. Ge, P. Wang, Y. Xing, Q. Yin, A. Wang, J. Shen, H. Lei, Z. Wang, and J. Wang, arXiv:2201.10352.
[59] Y.-B. Liu, J. Zhou, C. Wu, and F. Yang, Charge-4*e* superconductivity and chiral metal in 45°-twisted bilayer cuprates and related bilayers, Nat. Commun. **14**, 7926 (2023).
[60] J. Dukelsky, S. Pittel, and G. Sierra, Colloquium: Exactly solvable Richardson-Gaudin models for many-body quantum systems, Rev. Mod. Phys. **76**, 643 (2004).
[61] D. Lidsky, J. Shiraishi, Y. Hatsugai, and M. Kohmoto, Simple exactly solvable models of non-Fermi-liquids, Phys. Rev. B **57**, 1340 (1998).
[62] G. Baskaran, An exactly solvable fermion model: Spinons, holons and a non-Fermi liquid phase, Mod. Phys. Lett. B **5**, 643 (1991).